Radial Evolution of the Electron Velocity Distribution in the Heliosphere: Role of Collisions

S. Landi*, F. Pantellini† and L. Matteini†

*Dipartimento di Astronomia e Scienza dello Spazio, Università degli Studi di Firenze, Firenze, Italy
†LESIA, Observatoire de Paris, Paris, France

Abstract. The electron velocity distribution function in the solar wind has often been described as the superposition of an isotropic core, a moderately energetic and slightly anisotropic halo and a high energy field aligned beam. The relative weight of these components depends on the characteristics of the solar wind streams (fast and slow) and on the heliocentric distance. We present kinetic simulations using the model given in [1] to study the effects of electron-electron and electron-proton collisions on the electron velocity distribution function in the interplanetary space beyond ~ 0.3 AU from the Sun. We show that collisions do naturally generate a two population electron velocity distribution with an isotropic and cold "core" and a hot and collimated "halo". The temperature profiles and temperature anisotropies observed in our simulations are consistent with spacecraft observations [2, 3, 4]. Since waves are not included in our simulations we suggest that Coulomb collisions are an essential ingredient which should be included in any model of the evolution of the electron velocity distribution function in interplanetary space.

Keywords: Electron velocity distribution, Coulomb collisions, Solar wind, Numerical simulations
PACS: 96.50.Ci,52.65.-y,94.05.-a,52.25.Fi

INTRODUCTION

The solar wind electron velocity distribution function (eVDF) can generally be described as the superposition of two components [5, 6, 7]. 95% of the electrons constitute a relatively isotropic core and have energies below 50 eV. The remaining 5% constitute a high energy halo which has often been found to be appreciably anisotropic [5, 6, 7]. The halo anisotropy has been seen to increase with increasing wind speed [5, 6]. High core temperature anisotropies $(T_\parallel/T_\perp)_\mathrm{C} > 1.5$ positively correlated with high halo temperature anisotropies have been observed by ISEE 3 in rarefaction regions on the trailing edges of unusually tenuous high-speed streams [8]. Core and halo are often observed to have different velocities with the core drifting towards the Sun in the plasma rest frame [5]. Typical drift velocities are of the order 100 km/s in fast wind streams [5, 6, 7, 9]. Several attempts have been made to asses the radial electron temperature gradient at different radial distances, different heliographic latitudes and using data from various spacecrafts [see 2, for a review]. Ulysses in-ecliptic data inferred a power-law r^{β_C} for the core population and a power-law r^{β_H} for the halo population with $\beta_\mathrm{C} \simeq -0.85$ and $\beta_\mathrm{H} \simeq -0.38$ respectively [10]. Out-of-ecliptic Ulysses data give $-0.6 < \beta_\mathrm{C} < -0.4$, $-0.45 < \beta_\mathrm{H} < -0.26$ and $-0.86 < \beta_\mathrm{e} < -0.81$ for the total electron temperature [11, 2]. Ulysses data in the heliocentric distance range from 1.2 AU to 5.4 AU show a power-law decrease of the radial electron heat flux with exponent around 3.0 [10] and an intensity appreciably less than the classical Spitzer-Harm value [10, 3].

Arguments, both theoretical and experimental, suggest that (unlike the proton VDF) the eVDF can be significantly modulated by electron-electron and electron-proton collisions [12, 3]. In particular [3] showed that the electron temperature anisotropy is well correlated with the collisional age, i. e. with the estimated number of collisions suffered by an electron on its way from the Sun's corona to the spacecraft. [8] and [13] found a correlation between the core electron temperature anisotropy and both the core electron density and the plasma bulk velocity. These authors use a fluid description where the temperature anisotropy is regulated by the competition between adiabatic expansion and electron-electron collisions. However, their fluid model does not include the heat flux, which is has been measured by various spacecrafts. Fluid models are obviously unable to describe the eVDF. Similarly, in [14] a fluid model has been used to investigate the effect of Coulomb collisions on the core-halo drift velocity. On the other hand, simulations with test particles moving in a prescribed fluid background show a good agreement between the synthetic eVDF and Helios observations at 0.3 AU [15].

In previous works [1, 16] we used a fully kinetic model where fluid moments are computed directly from the particle's dynamics. The dynamics in the model is regulated by the external fields (gravitational and magnetic), a self-consistent macroscopic electrostatic field, and Fokker-Planck type collisions. The model has been successfully applied to the case of a bounded atmosphere [1] and has been shown to be able to simulate a solar type wind from

CP1216, *Twelfth International Solar Wind Conference*,
edited by M. Maksimovic, K. Issautier, N. Meyer-Vernet, M. Moncuquet, and F. Pantellini

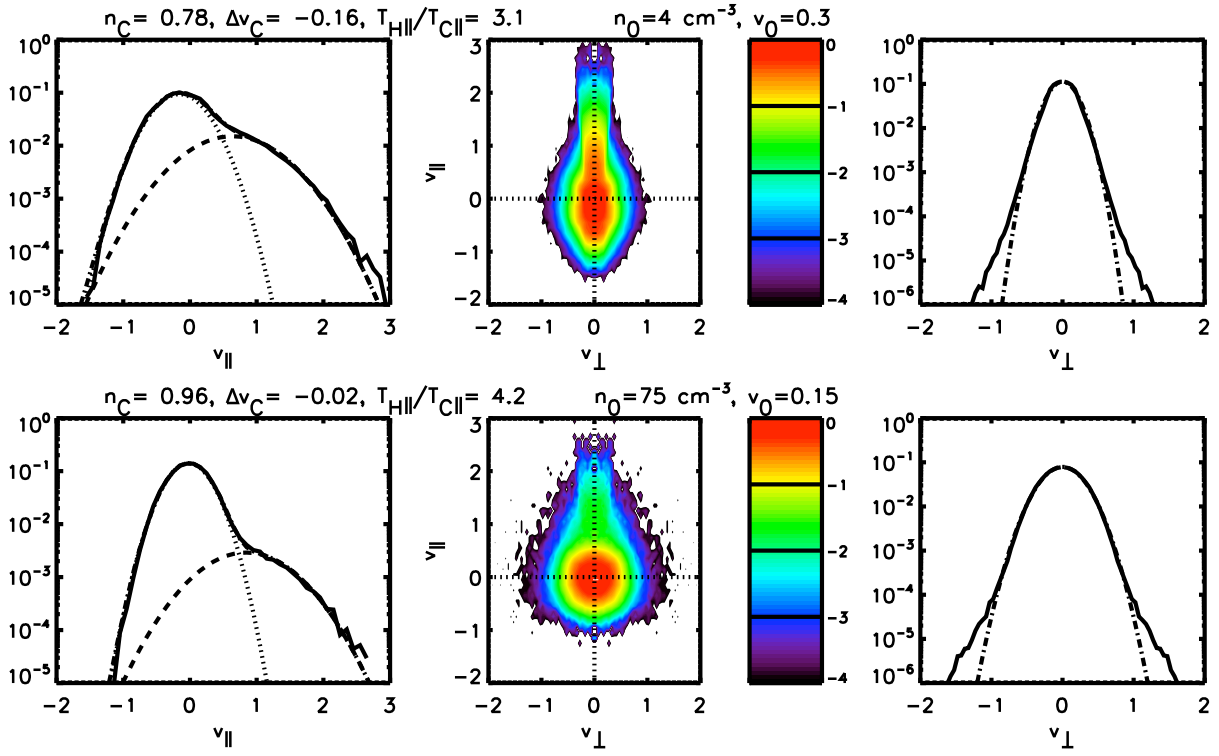

FIGURE 1. Electron velocity distribution functions for two simulations at $r \simeq 8.5 r_0$. Top and bottom panels refer to a dilute fast wind and a dense slow wind, respectively. n_C, Δv_C, and $T_{H\parallel}/T_{C\parallel}$ are the core densities, core velocities drift in the plasma frame, and halo-to-core parallel temperature ratios, respectively.

the subsonic to the supersonic regime [16].

In this contribution we present results obtained using the aforementioned kinetic model to describe the radial evolution of the solar wind eVDFs at distances beyond 0.3 AU from the Sun.

MODEL AND SIMULATION SETUP

Details of the model have been given elsewhere [1, 16] and will not be repeated in this note. Here, we shall merely recall that the model is based on the numerical integration of the equation of motion of an equal number N of electrons and protons. The particles are allowed to move freely in the spherical shell $r_0 < r < r_{\rm max}$, under the effect of a prescribed radial magnetic field $\mathbf{B} \propto \hat{r}/r^2$ and a self-consistent charge neutralizing electric field $\mathbf{E} = E(r)\hat{r}$ where $\hat{r} \equiv \mathbf{r}/r$ is the unit vector along the radial direction. We simulate shells of solar wind far enough from both the Sun and the acceleration region so that gravity can be neglected. Particles are tightened to the magnetic field by imposing magnetic moment conservation, i. e. $v_\perp^2/B = \text{const}$. Collisions are treated using a Fokker-Planck type prescription which has been discussed in Appendix B of [1].

We prescribe the VDF for both electrons and protons injected at the inner boundary at $r = r_0$ and $v_\parallel > 0$ to be given by drifting bi-Maxwellians

$$f_\alpha = \frac{\pi^{-3/2}}{v_{0\alpha\parallel} v_{0\alpha\perp}^2} \exp\left[-\frac{\left(v_\parallel - v_0\right)^2}{v_{0\alpha\parallel}^2} - \frac{v_\perp^2}{v_{0\alpha\perp}^2} \right] \qquad (1)$$

where $\alpha = \mathrm{e,p}$ designates the species, and where $v_{0\alpha\parallel,\perp}^2 \equiv 2T_{0\alpha\parallel,\perp}/m_\alpha$ are the thermal velocities in the parallel (radial) and perpendicular directions, respectively. Note that here, and throughout the remaining of the paper we assume that temperatures are systematically multiplied by the Boltzmann constant $k_{\rm B}$. Protons are supersonic everywhere within the simulated shell so that almost all protons escaping from the upper boundary at $r_{\rm max}$ will be re-injected into the system from the lower boundary r_0. On the contrary, electrons are subsonic and a significant fraction of those escaping from the upper boundary have to be re-injected back into the system from the upper boundary to ensure the equality of the proton and electron flux (zero current condition). Thus, the VDF for the electrons injected from the upper boundary is a drifting bi-Maxwellian with the same parallel and perpendicular temperatures as the outgoing electrons and drift velocity equal to proton drift velocity

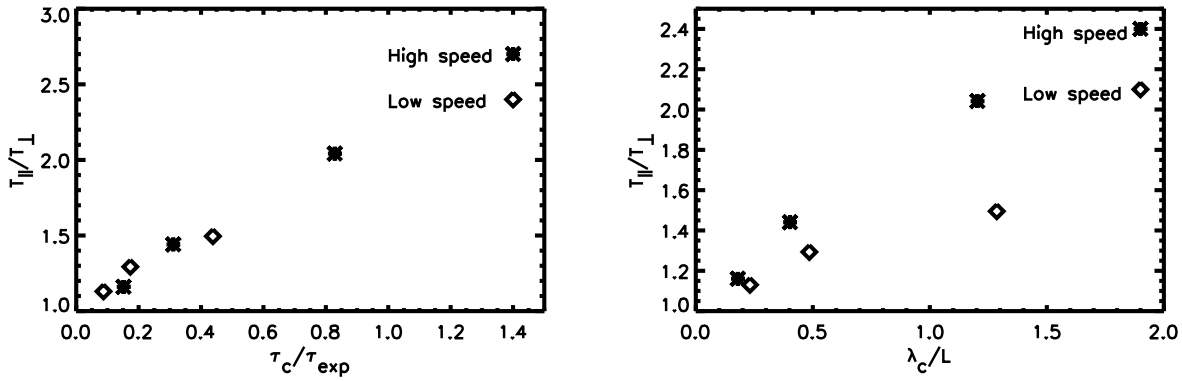

FIGURE 2. Core electron temperature anisotropy near $r \simeq 8\ r_0$ for high and low speed wind and various densities. In the left panel the measured temperature anisotropies are plotted against the collisional age as defined in Eq. (2). In the right panel the measured temperature anisotropies are plotted against the Knudsen number.

[see 16, for further details]. Once a stationary state has been reached, distribution functions and moments are obtained by regularly sampling the positions and velocities of all particles in the system.

We consider typical values for fast streams in the inner heliosphere near 0.3 AU, with a mean velocity $v_0 = 700$ km/s, a proton temperature $T_{0\mathrm{p}} = (T_{0\mathrm{p}\parallel} + 2T_{0\mathrm{p}\perp})/3 = 3\times10^5$ K [17] with anisotropy $A_\mathrm{p} = T_{0\mathrm{p}\perp}/T_{0\mathrm{p}\parallel} = 2$ [18], and an electron temperature $T_{0\mathrm{e}} = (T_{0\mathrm{e}\parallel} + 2T_{0\mathrm{e}\perp})/3 = 1.5\times10^5$ K.

As we are primarily interested in the radial evolution of the electron anisotropy we chose an isotropic eVDF $A_\mathrm{e} = T_{0\mathrm{e}\perp}/T_{0\mathrm{e}\parallel} = 1.0$ at the inner boundary at $r_0 \approx 0.3$ AU. With the given values of the electron and proton temperatures and assuming a typical density $n_0 \sim 10\ \mathrm{cm}^{-3}$, the Fokker-Planck electron collision frequency is $\nu_\mathrm{e} \approx 4\times10^{-5}\ \mathrm{s}^{-1}$, corresponding to an electron mean-free path of roughly 0.3 AU. The simulated system length is $L = r_{\max} - r_0 \approx 3$ AU.

Throughout the paper velocities are normalized to the parallel electron thermal velocity at r_0. In these units the bulk speed imposed at the boundaries is $v_0 = 0.3$ (corresponding to 700 km/s). Since our goal has been to measure the role of the expansion velocity versus the wind collisionality we have also performed slow wind simulations with $v_0 = 0.15$.

RESULTS

The 2D structure of the eVDF for a dilute fast wind (upper panels) and a dense slow wind (lower panels) is shown in Fig. 1. In both cases, the 2D distribution is seen to split into two populations consisting in a rather isotropic core and a a collimated "halo". The relative weight of the two populations has been measured by a fitting procedure assuming a sum of drifting bi-Maxwellians for the core and halo structure. The fitting parameters are the core and halo densities n_C and n_H, the drift velocities Δv_C and Δv_H in the plasma frame, the parallel ($T_{\mathrm{C}\parallel}$ and $T_{\mathrm{H}\parallel}$) and the perpendicular ($T_{\mathrm{C}\perp}$ and $T_{\mathrm{H}\perp}$) temperatures. Since the model distribution function depends non linearly on the above parameters we use the Levenberg-Marquardt fitting method [19] to extract their numerical values. The fitting shows that the core density is directly correlated with the collisionality of the system. Indeed, as n_0 increases or v_0 decreases, the ratio of the core density with respect the total density growths from about 0.78% to about 0.96%. Simultaneously, the core drift velocity decreases from -0.16 to -0.02. This is because as the ratio of the collision frequency ν_e to the inverse of the expansion time rises, a larger fraction of particles goes into the bulk of the distribution function. In addition, as Δv_H does not vary significantly between the slow and the fast wind simulations shown in Fig. 1, $|\Delta v_\mathrm{C}|$ must be smaller in the former case. The figure also shows that the halo-to-core temperature ratio growths as the total density increases. The left panels of Fig. 1 reveal the presence of suprathermal wings in the perpendicular direction. The strength of the wings appears to be inversely correlated with the system collisionality as the number of suprathermal electrons is larger in the fast and dilute case (top panels).

In Fig. 2 we report the measured core electron temperature anisotropy at a given distance for a set of 6 simulations with different densities n_0 and wind velocities v_0. The core electron temperature anisotropy appears to be mostly in the range 1.1 to 1.5 [8, 3]. In the left panel of the figure we have compared the temperature anisotropy with the inverse of the collisional age, i. e. with

$$\tau_\mathrm{c}/\tau_\mathrm{exp} = \frac{v_0}{L_0 \nu_\mathrm{e}} = K_\mathrm{e}\frac{v_0}{\nu_\mathrm{e}} \qquad (2)$$

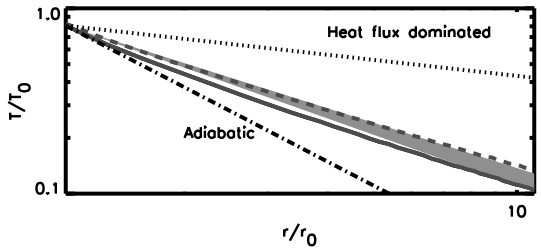

FIGURE 3. Mean electron temperature for two simulations with $n_0 = 75$ cm^{-3}: $v_0 = 0.3$ (solid) and $v_0 = 0.15$ (dashed). The gray region covers the range observed by the Ulysses spacecraft. The heat flux dominated and adiabatic power law profiles are given as a reference.

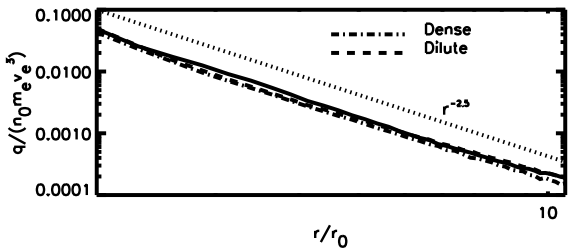

FIGURE 4. Normalized electron heat flux for the dense and dilute case for an expansion velocity $v_0 = 0.15$. The solid line is the collisionless heat flux based on [5, 21] with $\alpha = 1.5$ (see Eq. (3)) and the fitted values of $n_{\rm H}$, $\Delta v_{\rm H}$, $T_{\rm C\|}$ and $T_{\rm H\|}$ obtained for the simulation with $n_0 = 20$ cm^{-3}.

with $K_{\rm e}$ the electron Knudsen number (ratio between the mean free path and the macroscopic temperature length-scale), and $v_{\rm e}$ the local electron thermal velocity. The temperature anisotropy shows a clear "universal" correlation with the collisional age in a way very similar to what observed in space [3, 4]. The same correlation is lost when we compare the temperature anisotropy with the electron collisional depth, i. e. essentially the Knudsen number. In this case the anisotropy follows two different paths depending on the assumed expansion velocity.

The mean electron temperature profile is reported in Fig. 3 for two cases with $n_0 = 75$ cm^{-3} and different expansion velocities v_0. The temperature profiles do approximately follow a power law with an exponent in the range $\beta_{\rm e} = -0.8$ to -0.9 as inferred from Ulysses measurement (the gray region in the figure). The electron temperature profile is far from either the one-fluid adiabatic case with $\beta_{\rm e} = -4/3$ or even the heat flux dominated case with $\beta_{\rm e} = -2/7$ [e.g. 20].

The non-adiabatic radial profile of the electron temperature is the result of the presence of a strong heat flux. In Fig. 4 we report the measured heat flux profiles for two simulations with different densities and equal expansion velocities. The profiles do roughly follow a power law $\propto r^{-2.5}$. Also note that the per particle heat flux is almost identical in both simulations as already pointed out in [16]. Quite remarkably, in all the simulations performed, the heat flux is well described by the expression given in [5], viz.

$$q_{\rm e} = \alpha n_{\rm H} \Delta v_{\rm H} \left(T_{\rm H\|} - T_{\rm C\|} \right) \tag{3}$$

with α a constant of order of unity. The black curve in Fig. 4 is the computed heat flux using the obtained fitting parameters for the simulation with $n_0 = 20$ cm^{-3} and $v_0 = 0.15$.

DISCUSSION AND CONCLUSIONS

The evolution of the electron velocity distribution function has been studied using a fully kinetic code which includes Coulomb collisions in a Fokker-Planck type approximation [1, 16]. An initially isotropic eVDF has been let to evolve in an expanding supersonic wind. The high energy electron population coming from the lower boundary is collimated under the effect of the mirror force and results to be organized as a rather anisotropic "halo". The lower energy portion of the electrons is strongly subjected to Coulomb collisions and it has the tendency to buid-up a colder and more isotropic "core". The inflection point between the two population is regulated by Coulomb collisions: increasing the system density, i. e. reducing the mean-free-path, the inflection point on the eVDF moves towards higher velocities. The structure core-halo is also regulated by the insurgence of an electric field needed by the fact that the halo has the tendency to escape faster than the bulk protons. The effect of the electric field is to reduce the drift of the electrons and indirectly to increase the electron-proton collision frequency.

The characteristic densities, temperatures and drift velocities of the two populations correlate well with the collisionality of the system. In particular, the temperature anisotropy, which should increases monotonically during a collisionless expansion, is observed to be regulated by the ratio of the collision frequency to the inverse of the characteristic expansion velocity, in a way very similar to what observed in real solar wind data [3, 4]. This non-dimensional number contains the collisional properties (the Knudsen number) and the basic fluid parameters (thermal velocity and expansion velocity) which regulates the temperature anisotropy of an expanding plasma. The Knudsen number, which omits the dynamical parameter v_0, is not able to organize in a unique way the temperature anisotropy obtained in our simulations. Fig. 2 clearly shows that slow and fast wind

temperature anisotropies follow different path when plotted against the Knudsen number.

Synthetic eVDFs are in good qualitative and quantitative agreement with observed eVDFs [e. g. 5]. Although not introduced directly, we observe the development of non-thermal high energy wings in the perpendicular direction. The importance of such non-thermal features is inversely correlated with the system's collisionality. Given reasonable plasma parameters at 0.3 AU we find the radial evolution of both the electron temperature and the electron temperature anisotropy to be consistent with observations [2, 3, 4] under the effect of collisions only. This suggests that wave-particle interactions are not crucial in shaping the eVDF while waves have been shown to be important to the protons. The non-adiabatic evolution of the electron temperature is due to the presence of a strong collisionless heat flux which is mainly transported by the halo [21, 5]. The heat flux is seen to decrease roughly as $\propto r^{-2.5}$ which is slightly less than observed by Ulysses [e. g. 10].

Several issues should be addressed in further and more extended studies. For example, how much the inflection point as well as halo-core temperature ratios are organized by (1) collisions, (2) mirror force and (3) interplanetary electric field. Moreover, in this paper we have restricted our analysis to the supersonic region of the wind where gravitational forces may be neglected. It is possible that the extension of the simulation domain down into the subsonic region, where gravitational effects are dominant, does also play a role in shaping the evolution of the eVDF.

REFERENCES

1. S. Landi, and F. G. E. Pantellini, *Astron. Astrophys.* **372**, 686–701 (2001).
2. M. Maksimovic, S. P. Gary, and R. M. Skoug, *J. Geophys. Res.* **105**, 18337–18350 (2000).
3. C. Salem, D. Hubert, C. Lacombe, S. D. Bale, A. Mangeney, D. E. Larson, and R. P. Lin, *Astrophys. J.* **585**, 1147–1157 (2003).
4. Š. Štverák, P. Trávníček, M. Maksimovic, E. Marsch, A. N. Fazakerley, and E. E. Scime, *J. Geophys. Res. (Space Phys.)* **113**, 3103–+ (2008).
5. W. C. Feldman, J. R. Asbridge, S. J. Bame, M. D. Montgomery, and S. P. Gary, *J. Geophys. Res.* **80**, 4181–4196 (1975).
6. W. C. Feldman, J. R. Asbridge, S. J. Bame, J. T. Gosling, and D. S. Lemons, *J. Geophys. Res.* **83**, 5285–5295 (1978).
7. W. G. Pilipp, K.-H. Muehlhaeuser, H. Miggenrieder, M. D. Montgomery, and H. Rosenbauer, *J. Geophys. Res.* **92**, 1075–1092 (1987).
8. J. L. Phillips, J. T. Gosling, D. J. McComas, S. J. Bame, S. P. Gary, and E. J. Smith, *J. Geophys. Res.* **94**, 6563–6579 (1989).
9. W. G. Pilipp, K.-H. Muehlhaeuser, H. Miggenrieder, H. Rosenbauer, and R. Schwenn, *J. Geophys. Res.* **92**, 1103–1118 (1987).
10. E. E. Scime, S. J. Bame, W. C. Feldman, S. P. Gary, J. L. Phillips, and A. Balogh, *J. Geophys. Res.* **99**, 23401–23410 (1994).
11. K. Issautier, N. Meyer-Vernet, M. Moncuquet, and S. Hoang, *J. Geophys. Res.* **103**, 1969 (1998).
12. J. D. Scudder, and S. Olbert, *J. Geophys. Res. (Space Phys.)* **84**, 2755–2772 (1979).
13. J. L. Phillips, and J. T. Gosling, *J. Geophys. Res. (Space Phys.)* **95**, 4217–4228 (1990).
14. Y. Chen, R. Esser, and Y. Q. Hu, *J. Geophys. Res. (Space Phys.)* **108**, 1371–+ (2003).
15. Ø. Lie-Svendsen, V. H. Hansteen, and E. Leer, *J. Geophys. Res.* **102**, 4701–4718 (1997).
16. S. Landi, and F. G. E. Pantellini, *Astron. Astrophys.* **400**, 769–778 (2003).
17. R. Schwenn, *Large-Scale Structure of the Interplanetary Medium*, Springer-Verlag, 1990, vol. 1, pp. 99–181, 1 edn.
18. L. Matteini, S. Landi, P. Hellinger, F. Pantellini, M. Maksimovic, M. Velli, B. E. Goldstein, and E. Marsch, *Geophys. Res. Lett.* **34**, 20105 (2007).
19. D. W. Marquardt, *J. Soc. Indust. Appl. Math.* **11**, 431–441 (1963).
20. E. Leer, and W. I. Axford, *Sol. Phys.* **23**, 238–252 (1972).
21. J. V. Hollweg, *J. Geophys. Res.* **79**, 3845–3850 (1974).